Chapter 3

Al_2O_3 and Al_2O_3-ZrO_2 Fibers Obtained by Biotemplete with Low Thermal Conductivity

Tiago Delbrücke, Rogério A. Gouvêa,
Cristiane W. Raubach, Jose R. Jurado,
Faili C.T. Veiga, Sergio Cava, Mario L. Moreira and
Vânia C. Sousa

Additional information is available at the end of the chapter

http://dx.doi.org/10.5772/59011

1. Introduction

Certain porous materials have special properties and functions that cannot normally be obtained by conventional dense counterparts. Therefore, porous materials are now used in many applications such as final products and in various technological processes. Macroporous materials are used in various forms and compositions in everyday life; e.g. polymeric foams, packaging, lightweight aluminum structures in buildings, aircraft, and as a porous ceramic for water [1,2].

A growing number of applications that require advanced ceramics have appeared in recent decades, especially in environments where high temperatures, extended wear and corrosive environments are present. Such applications include the filtration of molten metals, high temperature insulation, support for catalytic reactions [3], filtration of particulates from exhaust gases of diesel engines and filtration of hot gases in various corrosive industrial processes, for example [4-6]. The advantages of using porous ceramic for these applications are generally a high melting point, suitable electronic properties, good corrosion resistance and wear resistance in combination with the characteristics acquired by the replacement of the solid material by voids in the component. Such characteristics include low thermal mass, low thermal conductivity, permeability control, high surface area, low density, high specific strength and a low dielectric constant [1,7]. These properties can be tailored for each specific application by controlling the composition and microstructure of the porous ceramic [8,9].

According to the type of application different microstructures and thus different preparation methods are required for porous ceramic bodies. For thermal or acoustic insulators materials with closed porosity are preferred, whereas membranes and filters require open pores with exactly defined pore size, for example. Are currently used some specific techniques to obtain pores with polymer and cotton for use in thermal insulation [10,11]. On the other hand, for application to environmental issues sodium hydroxide is used to pore formation [12].

This work uses a simple and versatile methodology to prepare sintered porous ceramic bodies obtained by replica method using organic fibers. The porous bodies of Al_2O_3 and Al_2O_3-ZrO_2 were synthesized through co-precipitation method [11] and replica [1,11] aiming to achieve a porous ceramic structure with thermal properties in agreement to the application of refractory materials.

2. Methodology

The Al_2O_3 fibers were prepared from an aluminum hydroxide slurry in which the organic fibers were dispersed and impregnated. The solvents were eliminated from the organic fibers through heat treatment and the remaining ceramic precursor was sintered to Al_2O_3.

The synthesis of aluminum hydroxide consisted of dissolving aluminum nitrate – $Al(NO_3)3.9H_2O$ (Synth) - in water; this solution was heated in a heating plate at 80°C. After its complete dilution ammonium hydroxide - NH_4OH (Vetec) - was added until pH = 9 was reached. The $Al(NO_3)$-NH_4OH ratio was 1:6 (in moles). Afterwards, anhydrous citric acid - $C_6H_8O_7$ (Synth) - was added until pH = 1 was reached, keeping a $Al(NO_3)$-$C_6H_8O_7$ molar ratio of 3:1. The addition of the citric acid causes the precipitation of aluminum nitrate in aluminum hydroxide - $Al(OH)_3$ - forming a slurry solution that was used to impregnate the organic fibers.

The organic fibers were impregnated in the aluminum hydroxide solution following the procedure of the replica method [1,11]. The organic fibers consisted of commercial cotton produced by Johnson & Johnson. After complete impregnation, the cotton fibers were pressed into a ceramic crucible to eliminate the surplus solution from the fibers and a green body with the shape of the recipient is obtained. These green bodies were placed on an electric oven (INTI, model FE-1300) for the calcination process, which occurred at 1200°C in air for 2 hours using a heating rate of 2°C/min. During this process there was a complete removal of the organic matter and α-alumina was formed from phase transition of aluminum hydroxide [13].

For the synthesis of zirconium hydroxide, initially, zirconium tetrachloride - $ZrCl_4$ (Synth) - was diluted in water. Next, this solution was heated in a heating plate at 80°C and after complete dilution ammonium hydroxide - NH_4OH-NH_4OH (Vetec) - was added until pH = 9 was reached keeping a $ZrCl_4$-NH_4OH molar ratio of 1:6. Afterwards, anhydrous citric acid - $C_6H_8O_7$ (Synth) - was added until pH = 1 was reached, keeping a $ZrCl_4$-$C_6H_8O_7$ molar ratio of 3:1. The addition of the citric acid causes the precipitation of zirconium tetrachloride in zirconium hydroxide - $Zr(OH)_4$ - forming a slurry solution that was used to impregnate the Al_2O_3 fibers.

http://dx.doi.org/10.5772/59011

The calcinated Al_2O_3 fibers were impregnated with the zirconium hydroxide slurry to form a structure of Al_2O_3 covered with ZrO_2. After impregnation, samples were sintered on the electric oven at 1200-1600°C in air for 4 hours using a heating rate of 2°C/min causing the transition of zirconium hydroxide to zirconia while the fibers are sintered [14].

2.1. Characterization

The crystalline phase was determined by X-ray diffraction (XRD) using a Shimadzu XRD-6000 diffractometer with CuKα; radiation at 40 kV and 40 mA with the patterns recorded in the 20 to 80 theta measuring range at a scan rate of 2°/min, at room temperature. Through micro-Raman was possible to verify the peaks corresponding to the symmetry of the ceramic phases; the analysis was performed in room temperature, using an wavelength of 514.5nm of an argon laser as exciting source. The energy was maintained in 15mW and a 50x lense was used. The spectra was registered through a monochromer T-64 Jobin-Yvon jointed to a CCD detector.

The morfology and structure of the pores created by the template of the metal oxides were analysed by FEG-SEM (Supra 35-VP, Carl Zeiss). Mean grain size was determined by using the intercept method.

A TG analysis of the porous alumina body was performed in a NETZSCH TG 209 F1 thermal analyzer using 10 mg samples heated to 25-900°C in air at a rate of 10°C/min.

Thermophysical properties are determined by the flash laser method [15-17] that allows to determine thermal diffusivity and specific heat of the sample. Specific heat and thermal diffusivity values were found through measurement of the increase in temperature of the opposite face of the material in the shape of a small disk, while the frontal face receives a strong energy flash by a laser. A laser with maximum power of 90 watts was applied. The irradiation time is within the order of 10 ms. The measurements were taken at room temperature in normal atmosphere.

The thermal diffusivity is calculated from the thickness of the sample and the required time for the temperature in the opposite face to reach 50% of the temperature in the laser incident face. Specific heat is determined by the density and thickness of the sample given the maximum temperature reached in the opposite face and the amount of heat received. Thermal conductivity is calculate by the product of the thermal diffusivity, specific heat and density, as shown in the equation 1 where K = thermal conductivity, α; = thermal diffusivity, ϱ; = density and C_p = specific heat.

$$K=\alpha \cdot \rho \cdot C_p \quad (1)$$

3. Results

Figure 1 shows the decomposition of organic fibers and aluminum hydroxide [18]. XRD patterns of samples in various temperatures suggest that phase changes occur at 200°C, 300°C,

400°C, 600°C, 700°C, 1100°C and 1600°C. The material phases agree with those phases obtained using the method of a solution precursor cation embedded in fibrous cotton organic matrix under high temperatures which profit from the reactive activity of decomposition and the reaction of fibers / aluminum hydroxide appears at 600°C but disappears at 700°C. At 700°C, the positions of all peaks agree with the positions of number 46-1212 of the JPCDS file (see Figure 1) which suggests that a completely crystallized Al_2O_3 product was obtained. A crystalline Al_2O_3 is obtained by the step-wise transition of $Al(OH)_3$ + cotton fibers between 300°C and 700°C. The results indicate that Al_2O_3 is the rhombohedral space group R-3C (167). Peaks were observed relative to α-Al_2O_3, and its crystalline peaks are identified in the X-ray diffractogram shown in Figure 1 as determined by the Scherrer equation [19], the average crystallite size is ~ 350 nm at 1600°C.

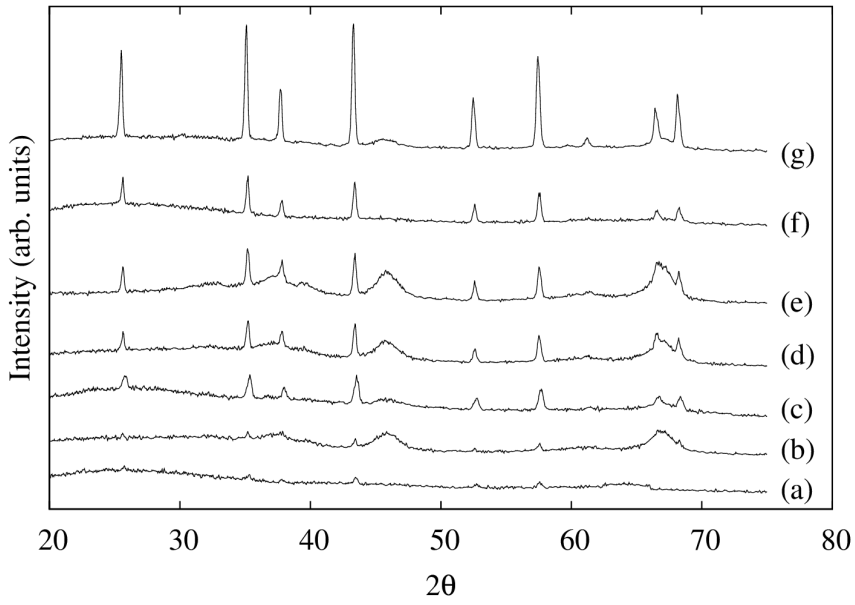

Figure 1. X-ray diffractogram of the Al_2O_3 porous bodies at temperatures of (a)200°C, (b)300°C, (c)400°C, (d)600°C, (e)700°C, (f)1100°C, (g)1600°C.

XRD of the sintered samples in different temperatures suggests the formation of alumina and zirconia phases in every temperature of sintering. The peaks for Al_2O_3-ZrO_2 are in agreement with those found in PDF (Powder Diffraction File) 53-559 file [20]; α-Al_2O_3 agrees with what is found in PDF 46-1212 file [21]; ZrO_2 agrees with the peaks in JPCDS 37-1484 file [22] (see Figure 2).

Raman is a powerful technique to detect the allotropic forms of zirconia [23]. According to the previous work of Popa et al [24], densified regions are caused by presence of monoclinic

http://dx.doi.org/10.5772/59011

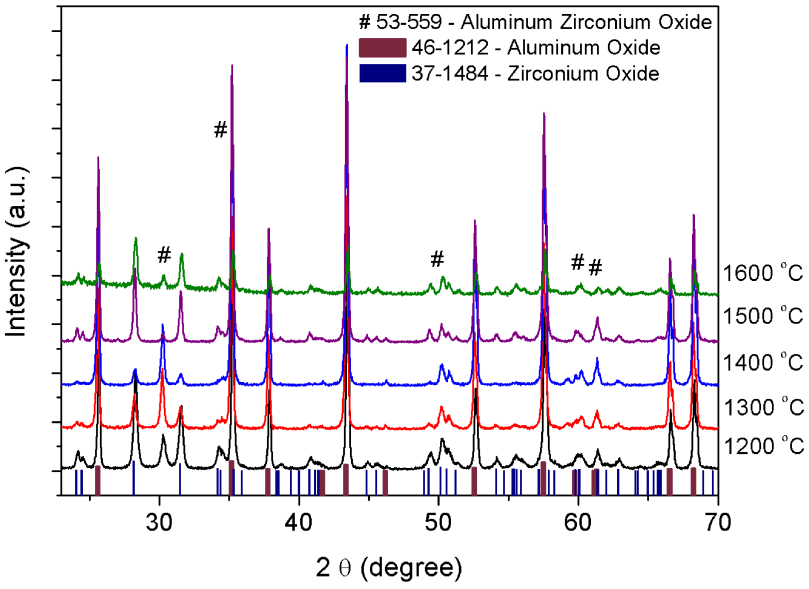

Figure 2. X-ray diffraction patterns of the Al_2O_3-ZrO_2 porous ceramics at several sintering temperatures.

zirconia. Figure 3 shows results regarding the measurements of micro-Raman spectroscopy dealing with wavelength radiation and vibration energies of the molecules. According to Raman results, vibration of Al-O bonds are related to the peaks described below: shows a peak at 378 cm-1, that may be considered polycrystalline α-Al_2O_3 [25]. For samples sintered above 1200°C there were significant spectroscopic bands in 410, 470, 605 and 630 cm^{-1}, which are identified as absorption bands characteristic of α-Al_2O_3 [26-28]. These results are agreement with the study conducted by Cava et al, in which spectroscopic bands of α-Al_2O_3 are present in temperatures above 1000°C [13].

Figure 4 shows the morphological profile of the Al_2O_3 and Al_2O_3-ZrO_2 porous body with an increase of 5000x where the samples are not similar. Densification and grain growth are two inversely proportional properties during the sintering process. The high porosity and low densification shown in SEM images of the Al_2O_3 porous bodies (Figure 4a) relates to a heating rate of 2°C/min which was used during the sintering process [29]. SEM micrographs (Figure 4b) show the presence of densified regions of zirconia; therefore, micro-Raman was used to identify the presence of monoclinic zirconia in these regions. Vibration of Zr-O bonds are related to the peaks on the spectroscopic bands of monoclinic zirconia were identified in frequencies of 505, 534, 550 cm^{-1} [24,30], peaks shown in temperatures of 1300-1600°C. Only a small amount of monoclinic zirconia is present; however it can be suggested that this amount was enough to densify the regions of porous ceramics agglomerating around grains [24]. Tetragonal zirconia was clearly detected in the peaks 260, 300, 323 and 340 cm^{-1} [24] increasing their intensity above 1300°C. It was found only two well defined peaks at 217 and 745

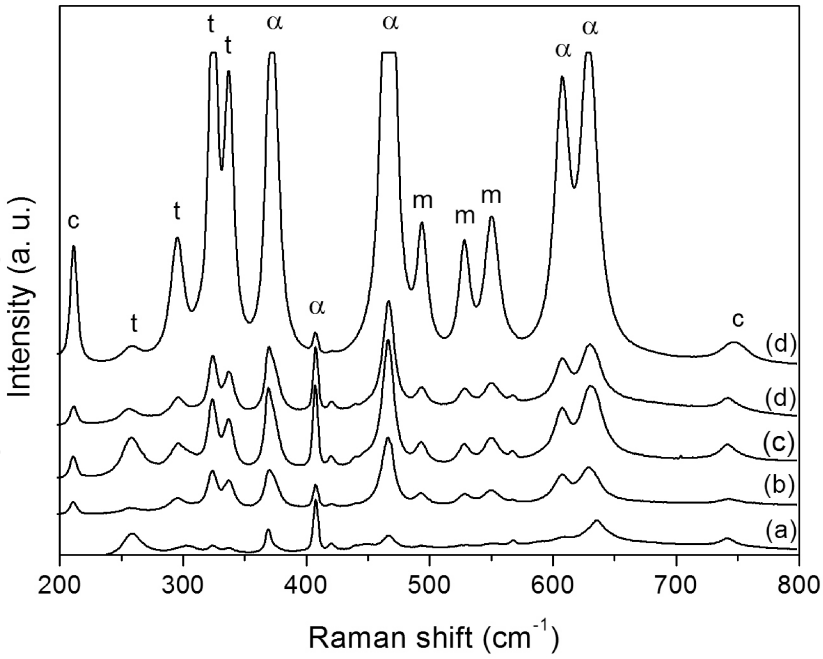

Figure 3. Micro-Raman spectra of the Al_2O_3-ZrO_2 porous ceramics at differents temperatures of: (a) 1200°C, (b) 1300°C, (c) 1400°C, (d) 1500°C and (e) 1600°C. α = α-alumina, c = cristobalite zirconia, t = tetragonal zirconia, m = monoclinic zirconia.

corresponding to cristobalite zirconia between temperatures of 1200-1600°C. The crystalline phase of Al_2O_3-ZrO_2 shown in Figure 2 has a cubic structure [20], not being detected by Raman.

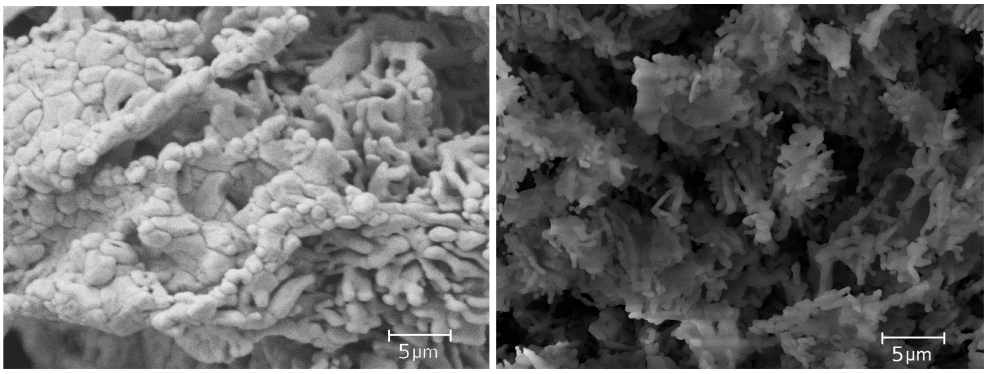

Figure 4. SEM micrographs of Al_2O_3 and Al_2O_3-ZrO_2 porous bodies at temperature of 1600°C at increasing of 5000x.

http://dx.doi.org/10.5772/59011

The method of embedding a cotton fiber in the organic matrix is based on the impregnation of a cellular structure with a ceramic suspension or solution precursor ceramic to produce a macroporous ceramic which has the same morphology as the original porous material (cotton) as illustrated in SEM images of Figure 4. Many cellular structures can be used as templates to produce macroporous ceramic embedding techniques for organic matrices.

The process of manufacturing ceramic fibers using cotton as a template by employing the embedding of the organic matrix [1] can be divided into two stages: the formation of the Al_2O_3 fiber morphology and the removal of the cotton used as a template.

The TG illustrated in Figure 5 shows the weight loss along with images of samples at temperatures ccurring in the formation of pore bodies at a temperature of 900°C; a gradual weight loss of weight is evident during the process. The sample weight loss was 82.5% up to 650°C where it terminated the decomposition of the carbonaceous mass with no significant loss of mass after the complete elimination of the carbonaceous mass.

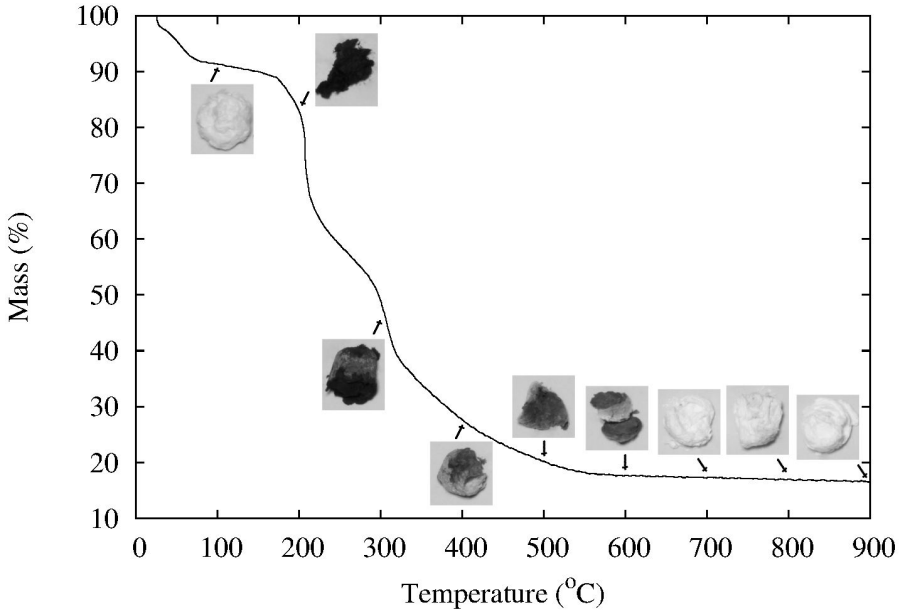

Figure 5. Thermogravimetric analysis of the Al_2O_3 porous bodies.

Al_2O_3 fibers are formed during the calcination process. After the formation of Al_2O_3 fibers, cotton models are removed through the decomposition process (see Figure 5) [31] which begins below 300°C, and terminates close to 700°C.

The porous body at 100°C has a weight loss of 9% which indicates that only evaporation solvents are used in the TG analysis. A weight loss of 8% over a primary loss of 9% at 200°C

indicates the evaporation of water in the sample and the beginning of the organic material evaporation. An additional weight loss of 55% at 400°C indicates the organic matter evaporation from the cotton fiber which forms the porous body [31]. A mass loss of 11% and a final weight of 83% in relation to the green body which indicates the total organic matter evaporation and the formation of the defined porous body.

Figure 4b shows morphological features of the porous ceramic of Al_2O_3-ZrO_2, in which grain growth was possible due to the presence of ZrO_2, causing the formation of diffusion barriers to control the growth and formation of the grain[32]. Furthermore, it was possible to verify the solid phase sintering, where the densification and grain growth are controlled by the diffusion across the grain boundary [33]. Therefore, it is reasonable to affirm that the formation of porosity in the structure is beneficial to decrease the thermal conductivity of the sample.

Table 1 illustrates physical and geometric properties of Al_2O_3 and Al_2O_3-ZrO_2 porous bodies.

Sample	Surface area (m^2/g)	Pore Volume (cm^3/g)	Pore Diameter (Å)	Porosity (%)
Al_2O_3	14.33	0.01	42.47	40.7
Al_2O_3-ZrO_2	8.45	0.006	4.19	77.9

Table 1. Physical and geometrical properties of the Al_2O_3 and Al_2O_3-ZrO_2 porous ceramics.

For the porosity calculation by the average of 3 samples, the Al_2O_3 theoretical density value was assumed to be 3940 $kg.m^{-3}$; the actual density was 2336 $kg.m^{-3}$. A porosity average value of 40.7% and 77.9% was obtained for the Al_2O_3 and Al_2O_3-ZrO_2 porous, respectively.

Table 2 shows the results of thermophysical property determinations of Al_2O_3 and Al_2O_3-ZrO_2 porous bodies.

Sample	a ($10^6 m^2 s^{-1}$)	($Kg.m^{-3}$)	C_p ($J.Kg^{-1}.K^{-1}$)	K ($W.m^{-1}.K^{-1}$)
Al_2O_3	1.24	2336	561.8	1.63
Al_2O_3-ZrO_2	1.09	2696	547.3	1.61

Table 2. Analysis of thermal conductivity by laser flash method of the Al_2O_3 and Al_2O_3-ZrO_2 porous bodies.

In the literature very few data about the thermal conductivity of the Al_2O_3 and ZrO_2 system is available. However the effect of the porosity to reduce the thermal conductivity of ceramic materials is a well recognized phenomenon, that has been widely applied for Al_2O_3 and ZrO_2 [3,10,34]. In addition to the absolute value of the porosity, the interconnection of grain size and pore shape have a significant influence on the final thermal conductivity. The high purity Al_2O_3 with no pores and with average grain size ~1 μm shows a thermal conductivity of approximately 33 $W.m^{-1}.K^{-1}$ at room temperature. High purity ZrO_2 without porosity and average grain size of ~1 μm has a thermal conductivity of approximately 3.3 $W.m^{-1}.K^{-1}$ [35] at

room temperature. Different studies show that thermal conductivity is independent of the grain size [36,37].

Some studies have been reported in the literature on the effect of porosity on reducing the thermal conductivity of solids, especially the porosity of Al_2O_3 [3,10]. In addition to its absolute value, the grain size and porous interconnectivity and shape have a significant influence on the final thermal conductivity. Porosity-free high-purity Al_2O_3 with a grain size ~1 μm has a thermal conductivity of approximately 33 $W.m^{-1}.K^{-1}$ at room temperature [35] which is very high when compared to the results obtained for porous Al_2O_3 reported by B. Nait-Ali et al [10] and Z. Zivcova et al [3]. Note that for the relative thermal conductivity the grain size dependence of thermal conductivity [36,37] is irrelevant, since it is cancelled out by taking the conductivity ratio [3].

Nait-Ali and co-workers [10] conducted a research on the Al_2O_3-ZrO_2 system relating thermal conductivity to porosity. Their samples were sintered at 1400°C and pores were generated by a pore-forming polymer. Results showed that commercial Al_2O_3 with 40% of porosity presented a thermal conductivity of 9 $W.m^{-1}.K^{-1}$ and average grain size of 0.5 μm; for commercial ZrO_2, thermal conductivity was 0.9 $W.m^{-1}.K^{-1}$ for 37% of porosity and average grain size of 0.1 μm.

The obtained Al_2O_3 porous bodies sintered at 1600°C have a thermal conductivity of 1.63 $W.m^{-1}.K^{-1}$ with a porosity of 40.71% and average grains size 0.55 μm, using cotton pore-forming agent and alumina obtained by a phase transition. Correlating these values and methods with literature data shows that Al_2O_3 porous bodies have high refractory properties from the combination of factors such as the synthesis method, grain size and porosity, when compared to the thermal conductivity of alumina bodies analyzed at temperatures as high as 1000°C [38].

Bansal and co-workers [39], using samples of commercial ZrO_2-Al_2O_3 sintered at 1000°C with density around 99% with average grain size of ~1 μm showed a thermal conductivity of 6.9 $W.m^{-1}.K^{-1}$. The porous Al_2O_3-ZrO_2 fibers obtained in this work were sintered at 1600°C and the calculated thermal conductivity was 1.61 K($W.m^{-1}.K^{-1}$) with a porosity of 77.9% and an average grain size of ~1 μm. The cotton replicated fibers of Al_2O_3-ZrO_2 sintered at 1600°C presented very low thermal conductivity compared to other works using different processes of pore formation.

4. Conclusions

Al_2O_3 porous bodies composed of ceramic fibers were successfully obtained by the embedded fibrous organic matrix method with cotton as a template. SEM at different temperatures during heat treatment along with thermogravimetric analysis data indicates a step-by-step method for the complete formation of the ceramic fiber porous body. The sintering temperature, low heating rate and the use of cotton as template had a strong effect on the surface area, pore size and distribution of the synthesized fibers. Thermal conductivity data show excellent results when compared to the literature, due to the direct influence of the organic template as a shape-

model and the efficient method of synthesis. The results show that the Al_2O_3 and Al_2O_3-ZrO_2 porous body are an excellent thermal insulator with direct application for refractories. A higher porosity and lower densification of the porous body is made possible with the addition of ZrO_2 to the Al_2O_3 matrix. However, there was no difference in thermal conductivity due to the characteristic values of density, specific heat and microstructure observed in both materials.

Author details

Tiago Delbrücke[1], Rogério A. Gouvêa[1], Cristiane W. Raubach[1], Jose R. Jurado[1], Faili C.T. Veiga[1], Sergio Cava[1], Mario L. Moreira[2] and Vânia C. Sousa[3]

1 Graduate Program in Science and Materials Engineering, Technology Development Center, Federal University of Pelotas, Pelotas, Brazil

2 Institute of Physics and Mathematics, Federal University of Pelotas, Pelotas, Brazil

3 Engineering Materials Department, Federal University of Rio Grande do Sul, Porto Alegre, Brazil

References

[1] Studart, A., Gonzenbach, U., Tervoort, E. & Gauckler, L. (2006). Processing routes to macroporous ceramics: a review, J. Am. Ceram. Soc. 89(6): 1771-1789.

[2] Ohji, T. & Fukushima, M. (2012). Macro-porous ceramics: processing and properties, Int. Mater. Rev. 57(2): 115-131.

[3] Zivcova, Z., Gregorova, E., Pabst, W., Smith, D., Michot, A. & Poulier, C. (2009). Thermal conductivity of porous alumina ceramics prepared using starch as a pore-forming agent, J. Eur. Ceram. Soc. 29(3): 347-353.

[4] Okada, K., Shimizu, M., Isobe, T., Kameshima, Y., Sakai, M., Nakajima, A. & Kurata, T. (2010). Characteristics of microbubbles generated by porous mullite ceramics prepared by an extrusion method using organic fibers as the pore former, J. Eur. Ceram. Soc. 30(6): 1245-1251.

[5] Okada, K., Uchiyama, S., Isobe, T., Kameshima, Y., Nakajima, A. & Kurata, T. (2009). Capillary rise properties of porous mullite ceramics prepared by an extrusion method using organic fibers as the pore former, J. Eur. Ceram. Soc. 29(12): 2491-2497.

[6] Okada, K., Imase, A., Isobe, T. & Nakajima, A. (2011). Capillary rise properties of porous geopolymers prepared by an extrusion method using polylactic acid (PLA) fibers as the pore formers, J. Eur. Ceram. Soc. 31(4): 461-467.

[7] Schacht, C. (2004). Refractories handbook, Vol. 178, CRC.

[8] Dong, Q., Su, H., Xu, J., Zhang, D. & Wang, R. (2007). Synthesis of biomorphic ZnO interwoven microfibers using eggshell membrane as the biotemplate, Mater. Lett. 61(13): 2714-2717.

[9] Dong-Dong, W., Gang, W., Xiao-Fei, S., Ya-Ping, L., Shu-Qiang, D. & Hong-Xia, L. (2012). Fabrication of nanoporous mullite ceramics, Chinese J. Inorg. Chem. 28(3): 491-494.

[10] Nait-Ali, B., Haberko, K., Vesteghem, H., Absi, J. & Smith, D. (2007). Preparation and thermal conductivity characterisation of highly porous ceramics: Comparison between experimental results, analytical calculations and numerical simulations, J. Eur. Ceram. Soc. 27(2-3): 1345-1350.

[11] Delbrücke, T., Gouvea, R. A., Moreira, M. L., Raubach, C. W., Varela, J. A., Longo, E., Gonçalves, M. R. & Cava, S. (2012). Sintering of porous alumina obtained by biotemplate fibers for low thermal conductivity applications, Journal of the European Ceramic Society.

[12] Bento, A. C., Kubaski, E. T., Sequinel, T., Pianaro, S. A., Varela, J. A. & Tebcherani, S. M. (2013). Glass foam of macroporosity using glass waste and sodium hydroxide as the foaming agent, Ceramics International 39(3): 2423-2430.

[13] Cava, S., Tebcherani, S., Souza, I., Pianaro, S., Paskocimas, C., Longo, E. & Varela, J. (2007). Structural characterization of phase transition of Al_2O_3 nanopowders obtained by polymeric precursor method, Mater. Chem. Phys. 103(2-3): 394-399.

[14] Ussui, V., Leitão, F., Yamagata, C., Menezes, C. A., Lazar, D. R. & Paschoal, J. O. (2003). Synthesis of ZrO_2-based ceramics for applications in sofc., Materials science forum, Vol. 416, pp. 681-686.

[15] Parker, W., Jenkins, R., Butler, C. & Abbott, G. (1961). Flash method of determining thermal diffusivity, heat capacity, and thermal conductivity, Jpn. J. Appl. Phys. 32(9): 1679-1684.

[16] Taylor, R. (1979). Heat-pulse thermal diffusivity measurements, High Temp.- High Pressures 11(1): 43-58.

[17] Ferreira, R., Miranda, O., Dutra Neto, A., Grossi, P., Martins, G., Reis, S., Alencar, D., Soares Filho, J., Lopes, C. & Pinho, M. (2002). Implantação no CDTN de laboratório de medição de propriedades termofísicas de combustíveis nucleares e materiais através do método flash laser, 2002 International Nuclear Atlantic Conference-INAC 2002, pp. 11-16.

[18] Deng, Z., Fukasawa, T., Ando, M., Zhang, G. & Ohji, T. (2001). High-surface-area alumina ceramics fabricated by the decomposition of al (oh) 3, J. Am. Ceram. Soc. 84(3): 485-491.

[19] Cullity, B. & Stock, S. (1972). Elements of X-ray Diffraction, Vol. 170, Prentice Hall.

[20] Kimmel, G., Zabicky, J., Goncharov, E., Mogilyanski, D., Venkert, A., Bruckental, Y. & Yeshurun, Y. (2006). Formation and characterization of nanocrystalline binary oxides of yttrium and rare earths metals, Journal of alloys and compounds 423(1-2): 102-106.

[21] Maslen, E., Streltsov, V., Streltsova, N., Ishizawa, N. & Satow, Y. (1993). Synchrotron x-ray study of the electron density in-Al_2O_3, Acta Crystallographica Section B: Structural Science 49(6): 973-980.

[22] McMurdie, H. F., Morris, M. C., Evans, E. H., Paretzkin, B., Wong-Ng, W. & Hubbard, C. R. (1986). Methods of producing standard x-ray diffraction powder patterns, Powder Diffraction 1(01): 40-43.

[23] Kakihana, M., Yashima, M., Yoshimura, M., Borjesson, L. & Mikael, K. (1993). Application of raman spectroscopy to phase characterization of ceramic hightc superconductors and zirconia related materials, Resesarch Trends (1): 261-311.

[24] Popa, M., Kakihana, M., Yoshimura, M. & Calderón-Moreno, J. M. (2006). Zircon formation from amorphous powder and melt in the silica-rich region of the alumina-silicazirconia system, Journal of non-crystalline solids 352(52): 5663-5669.

[25] Watson, G., Daniels, W. & Wang, C. (1981). Measurements of raman intensities and pressure dependence of phonon frequencies in sapphire, Journal of Applied Physics 52(2): 956-958.

[26] Nagabhushana, K., Lakshminarasappa, B. & Singh, F. (2009). Photoluminescence and raman studies in swift heavy ion irradiated polycrystalline aluminum oxide, Bulletin of Materials Science 32(5): 515-519.

[27] Boumaza, A. & Djelloul, A. (2010). Estimation of the intrinsic stresses in α-alumina in relation with its elaboration mode, Journal of Solid State Chemistry 183(5): 1063-1070.

[28] Mariotto, G., Cazzanelli, E., Carturan, G., Di Maggio, R. & Scardi, P. (1990). Raman and x-ray diffraction study of boehmite gels and their transformation to α- or β-alumina, Journal of Solid State Chemistry 86(2): 263-274.

[29] Zhou, Y., Hirao, K., Yamauchi, Y. & Kanzaki, S. (2004). Densification and grain growth in pulse electric current sintering of alumina, J. Eur. Ceram. Soc. 24(12): 3465-3470.

[30] Boullosa-Eiras, S., Vanhaecke, E., Zhao, T., Chen, D. & Holmen, A. (2011). Raman spectroscopy and x-ray diffraction study of the phase transformation of ZrO_2-Al_2O_3 and CeO_2-Al_2O_3 nanocomposites, Catalysis Today 166(1): 10-17.

[31] Fan, T., Sun, B., Gu, J., Zhang, D. & Lau, L. (2005). Biomorphic Al_2O_3 fibers synthesized using cotton as bio-templates, Scr. Mater. 53(8): 893-897.

[32] Caruso, F., Caruso, R. & Möhwald, H. (1998). Nanoengineering of inorganic and hybrid hollow spheres by colloidal templating, Science 282(5391): 1111.

[33] Bernard-Granger, G. & Guizard, C. (2008). New relationships between relative density and grain size during solid-state sintering of ceramic powders, Acta Materialia 56(20): 6273-6282.

[34] Nait-Ali, B., Haberko, K., Vesteghem, H., Absi, J. & Smith, D. (2006). Thermal conductivity of highly porous zirconia, Journal of the European Ceramic Society 26(16): 3567-3574.

[35] Pabst, W. & Gregorová, E. (2007). Effective thermal and thermoelastic properties of alumina, zirconia and alumina-zirconia composite ceramics, New Developments in Materials Science Research pp. 77-137.

[36] Smith, D., Fayette, S., Grandjean, S., Martin, C., Telle, R. & Tonnessen, T. (2003). Thermal resistance of grain boundaries in alumina ceramics and refractories, Journal of the American Ceramic Society 86(1): 105-111.

[37] Smith, D., Grandjean, S., Absi, J., Kadiebu, S. & Fayette, S. (2003). Grain-boundary thermal resistance in polycrystalline oxides: alumina, tin oxide, and magnesia, High Temperatures-High Pressures 35(1): 93-100.

[38] Taylor, R. & Dos Santos, W. (1993). Effect of porosity on the thermal conductivity of alumina, High Temp.- High Pressures 25: 89-98.

[39] Bansal, N. & Zhu, D. (2005). Thermal conductivity of zirconia-alumina composites, Ceramics international 31(7): 911-916.

INTECH